Environmental Science and Pollution Research (2021) 28:18589–18603
https://doi.org/10.1007/s11356-020-11153-9

RECENT ENVIRONMENTAL GEOCHEMICAL TRENDS

# Facile fabrication of green nano pure $CeO_2$ and Mn-decorated $CeO_2$ with *Cassia angustifolia* seed extract in water refinement by optimal photodegradation kinetics of malachite green

Dhivya Antony[1] · Rakhi Yadav[1]

Received: 28 May 2020 / Accepted: 5 October 2020 / Published online: 10 October 2020


## Abstract

To eradicate the aquatic pollution caused by dyes, trendily the global researchers provide dedication to dye degradation using nanostructured photocatalyst. This research work is dedicated to explore an advanced, facile, bio-compact green fabricated nanostructure for water refinement. In this regard, plant-mediated syntheses of pure $CeO_2$ and Mn-decorated $CeO_2$ nanopowders have been inspected using seed extract of *Cassia angustifolia*. Investigations through UV-diffuse reflectance spectroscopy explored the significantly tuned band gap of Mn:$CeO_2$. FT-IR spectroscopy shows the existing functional groups of high-potential phenolic compounds, proteins, and amino acids in *Cassia angustifolia* act as reducing and capping agents involved in the green fabricated nanostructured samples. X-ray diffraction pattern has been exposed to crystalline cubic fluorite morphology in a single phase and it leads to a regulated optimized amount of Mn on $CeO_2$ nanostructure. The FESEM analysis predicts the morphology of $CeO_2$ in spherical and Mn:$CeO_2$ in flower-like structure. The HRTEM analysis has portrayed particle size of $CeO_2$ is 11 nm and tuned Mn:$CeO_2$ nanostructure is 9 nm. The HRTEM images revealed the average particle size in the range 10–12 nm in $CeO_2$ and 8–9 nm in 5 mol% Mn:$CeO_2$ nanoparticles. It showed a decrease in average particle size with an increase in Mn concentration and the reduction in size may be due to the replacement of Ce(IV) with Mn(II) ions. The elemental composition in nanostructure was predicted using energy-dispersive X-ray analysis. The rapid photocatalytic degradation efficiency of malachite green was effectually performed and compared with the kinetics model of Mn:$CeO_2$ and pure $CeO_2$ nanostructures. From the augmented results, tuned Mn:$CeO_2$ was found to act as the finest green fabricated photocatalyst in the amputation of lethal and carcinogenic dye.

**Keywords** Green nano-synthesis · Pure $CeO_2$ · Mn-decorated $CeO_2$ · *Cassia angustifolia* · Malachite green · Degradation

## Introduction

In the modern ecosystem, water pollution by organic dyes is one of the firmest methods to be compensated by eco-friendly purification techniques using nano-photocatalyst (Wang et al. 2012; Higashimoto et al. 2013). Nano-photocatalyst synthesized by a novel green method using plants produces better results due to virtuous physical and chemical properties capable of degrading the dye without generating the least inferior pollutant (Nagajyothi et al. 2019). The cationic triphenylmethane dye—malachite green (MG)—was assets for its obstinate highly toxic, mutagenic, and carcinogenic nature. They rampantly bid in numerous trades and productions like textile, food, paper, leather, ceramics, and agronomic industry by acting as a blushing agent (Mohamed et al. 2019). Consequently, photodegradation was fascinated to eradicate toxic dye in the aquatic physique amid different methods to shield the environment from dye pollutants (Feizpoor et al. 2019). The unique rich properties of semiconducting cerium(IV) oxide $CeO_2$ with 3.2 eV band gap were widely reviewed due to their probable applications and strong antioxidant properties subsequent to the photocatalytic absorber capability of titanium oxide and zinc oxide (Herrling et al. 2013).

doped cerium oxide nanoparticles: enhanced

Responsible Editor: Sami Rtimi

✉ Rakhi Yadav
rakhiyadavres@yahoo.co.in

[1] Department of Chemistry, Madras Christian College, University of Madras, East Tambaram, Chennai, Tamil Nadu 600 059, India

Inspected nanomaterial $CeO_2$ was used for ecological water pollutant prohibition and photocatalytic progression due to its stability and non-hazardous nature. Nanocomposites and metal-doped $CeO_2$ take initiate tenders in different extents such as optical devices (Goubin et al. 2004), UV absorbents and filters (Li et al. 2002; Truffault et al. 2010), gas sensors (Van Dao et al. 2019), and photocatalysis (Gnanam and Rajendran 2018; Li et al. 2012). To improve the photocatalytic activity of $CeO_2$, surface defect was apprise to rush the electrons and avert the recombination of electron and holes and act as a spot for adsorbing dye molecules. Based on the literature survey, the physical properties of $CeO_2$ were altered by tapering the band gap of $CeO_2$ nanoparticles which impart with metal ions like Mn (Prabaharan et al. 2018), heterostructure-based semiconducting material such as $TiO_2$/$CeO_2$ (Lu et al. 2016; Pavasupree et al. 2005), and nonmetal N-doped $CeO_2$ (Mao et al. 2008; Zhou et al. 2005) nanoparticles by chemical approach quantifying the photocatalytic action of $CeO_2$.

Recently, decorating the surface of metal oxide nanoparticles with metal nanoparticles has arisen to alter the properties and surface behavior of metal oxide nanoparticles by electrons incline with amazing photocatalytic potential. The surface decoration $CeO_2$ by Mn was inspired as an effective method to hinder the recombination of photogenerated $CeO_2$, where 3*d* transition metal Mn occurs in the bivalence oxidation state and takes the extremely potent in letting substantial optical absorption by primer transitional bands inside the forbidden gap (Murugan et al. 2005; Pavan Kumar et al. 2014). In this work, the catalytic nature of green nano-$CeO_2$ was compelled with Mn metal ions due to the accessible energy dropping level of empty *d* orbitals compared to 4 *f* orbitals which can easily allocate the oxygen species generated by the electrons of adsorbed molecules (Yue and Zhang 2009; Montini et al. 2016).

In modern research, to stun the hazardous chemical synthesis, dye removal was done using plant-mediated nanoparticles (Bodaiah et al. 2018; Sijo Sijo et al. 2017; Tanur and Ahmaruzzaman 2015; Behrouz et al. 2019). Concerning these literature reports, the green nano-$CeO_2$ and Mn:$CeO_2$ photocatalysts were prepared for the first time in the green approach using *Cassia angustifolia* seed whose gum acts as an effective natural coagulant for eradicating dyes, which can be the best ancillary for using chemicals in wastewater treatment (Rashmi Rashmi et al. 2002). The seed extracts rich in carbohydrates, proteins, and fatty acids which act as natural surfactants give high stable nanoparticles (Manjoosha et al. 2010; Shabina et al. 2016) and have an ability to reduce the metal ion to high stable nanoparticles (Dhivya et al. 2020).

Facile green synthesized nano-$CeO_2$ and nano-Mn-decorated $CeO_2$ photocatalysts were characterized with a minimum nanosized flower-like morphology and compared with Cassia seed and conventional synthesized $CeO_2$, Mn:$CeO_2$ nanoparticles. The photocatalytic activity of green synthesized nano-$CeO_2$ and nano-Mn-decorated $CeO_2$ (Mn:$CeO_2$) photocatalysts was carried out in dark, visible, and UV sunlight and among them, UV radiation results were good on cationic malachite green dye solution and the kinetics study was predicted. To explore the potential of a photocatalyst, the dye degradation efficiency was compared with green fabricated $CeO_2$ and tuned Mn:CeO2 nano-powders. This study aimed to synthesize effective green nano-photocatalyst which shows highly efficient decoloration in a short duration.

## Experimental details

### Needed materials

Ammonium ceric sulfate dihydrate ($(NH_4)_4$ Ce $(SO_4)_4$ $2H_2O$, 99%), manganese sulfate monohydrate ($MnSO_4$ $H_2O$, 99%), malachite green (molecular formula: $C_{52}H_{54}N_4O_{12}$, molecular weight: 927.02 g/mol, $\lambda_{max}$ = 620 nm), and ethanol were purchased from LOBA Chemie, India. The needed solutions for experimental work were prepared using double-distilled deionized water. Fresh dried seeds of *Cassia angustifolia* were collected from the cultivated area of Katambur situated in the zone of Tuticorin, Tamil Nadu, India.

### Preparation of seed extract

The impurities present in the collected seed materials were purified by washing and drying in shade. In a beaker, 100 ml of double-distilled water with 5 g of fine powdered *Cassia angustifolia* seed was assorted and simmered for 10 min in the heating mantle at 70 °C. Then, the mixture was chilled and sieved using Whatman No. 1. The clear sterile filtrate was stored and used for the facile green synthesis.

### Fabrication of $CeO_2$ nano-powders

In a conical flask, 70 ml of 0.1 M ammonium ceric sulfate dihydrate was prepared and placed on the magnetic stirrer with a hot plate at 70 °C. To the aqueous cerium salt solution, 30 ml of *Cassia angustifolia* seed extract was added and uniformly stirred for an hour to attain a yellow colloidal solution. Then, the solid product was obtained by centrifuging at 2000 rpm for 10 min and cleaned with distilled water and ethanol to eradicate the impurities. The powdered $CeO_2$ NPs were attained by heating the precipitate in a microwave oven at 2.45 GHz for 15 min.

### Fabrication of Mn-decorated $CeO_2$ nano-powders

To prepare Mn-decorated $CeO_2$ nano-powders, initially, $CeO_2$ was synthesized thrice using the abovementioned process

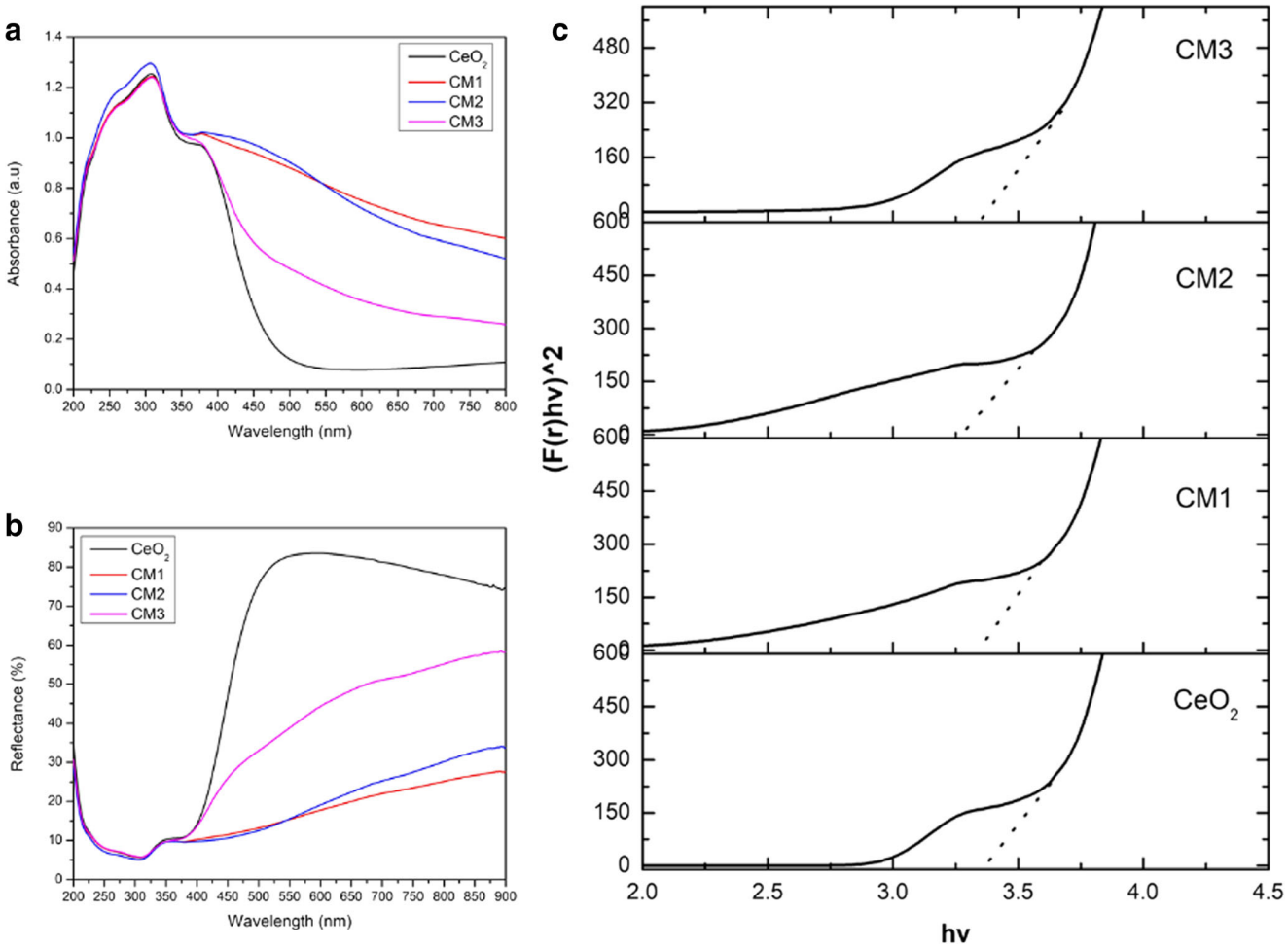


**Fig. 1** **a** UV-DRS absorbance spectra of $CeO_2$, CM1, CM2, and CM3. **b** Reflectance spectra of $CeO_2$, CM1, CM2, and CM3. **c** The plot of $(F(r)\ h\nu)^2$ against hν

with slight variation in Ce precursor up to the formation of yellow colloidal suspension, and different Mn contents CM1 (2.5 mol%), CM2 (5.0 mol%), and CM3 (7.5 mol%) were added by the deposition process. The resultant mixture Mn:$CeO_2$ was continuously stirred for an hour and the colloidal solution was centrifuged and washed with distilled water and ethanol to get rid of the impurities. The powdered Mn:$CeO_2$ NPs were attained by heating the precipitate in a microwave oven at 2.45 GHz for 15 min.

## Required characterization

The properties of green fabricated $CeO_2$ and Mn:$CeO_2$ nano-powders were examined by analytical techniques. The optical properties were monitored by UV–visible diffuse reflectance spectra JASCO V-600 spectrophotometer. The functional groups on the surfaces of the nano-powders like secondary metabolites in plant source and decorated metal can be predicted by Nicolet iS5 model Fourier transform infrared spectrometer (FT-IR) with KBr technique in the 400–4000 $cm^{-1}$ range. The phase and crystalline nature of particles were noted using X-ray powder diffraction (PANalytical X'pert PRO model) CuKα ($\lambda = 1.5406$ Å) radiation. To ration the stability, particle distribution pattern and zeta potential were calculated by scattering and sonicating the samples in Milli-Q water using Nanopartica SZ-100, Horiba Scientific. Field emission scanning electron microscope with energy-dispersive X-ray (EDAX) (JEOL-JSM-6700F) instrument operated at 5 kV for $CeO_2$, scanning electron microscopy (FEI Quannta FEG200), and HRTEM with EDAX (TEM-2100 plus electron microscope) shows the morphologies and size of the synthesized samples.

## Determination of malachite green degradation

The photodegradation of the organic cation dye malachite green (MG) bluish-green color in water exhibits peak at 620 nm. The photocatalytic activity of green fabricated $CeO_2$ and Mn:$CeO_2$ (CM2) nano-powders optimizes the degradation parameters for Malachite green. The photocatalytic reactions were carried out in different radiation by exposing the reaction chamber in visible, UV, and direct sunlight. A

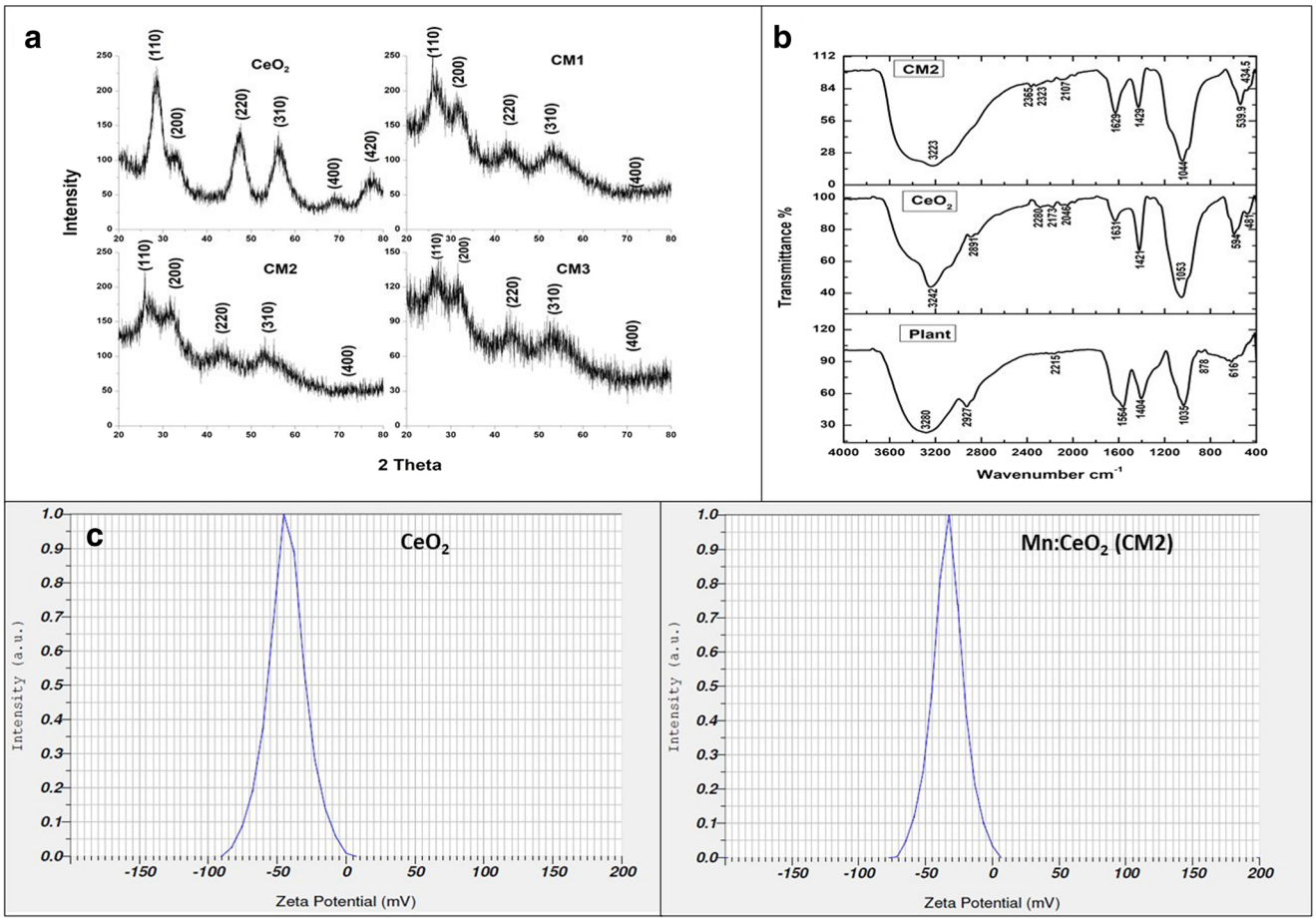


**Fig. 2** **a** XRD spectra of $CeO_2$, CM1, CM2, and CM3. **b** FT-IR of plant, $CeO_2$, and CM2. **c** Zeta potential of $CeO_2$ and CM2

stock solution of MG was made by liquefying the 0.1 g of MG into a 1-l volume of deionized water. The chosen concentrations of dye solutions required for the degradation process were diluted from the stock solution of MG. The amputation of malachite green from solution was determined by capturing visible, UV sunlight. The radiation was regulated by using a normal LED lamp with 7 W for visible radiation, a UV bulb with 30 W for UV radiation, and direct sunlight. During the radiation time, the dye solution with the required photocatalyst was positioned with the nearest contact. The durable color of the solution was calibrated to get the decoloration efficiency to fix the light source. In the extant situation, aqueous *Cassia angustifolia* seed extract, $CeO_2$, and the dopant Mn ions on $CeO_2$ nanomaterials prime to degrade the dye solution. Since the coagulant nature of *Cassia angustifolia* seed gum acts as a substituent of chemical coagulant, the dye removing efficiency was carried out by using seed extract. To sign the degrading efficiency, seed was applied in varied percentages (1%, 3%, 5%, 7%, and 9%) to reduce the malachite green dye solution of 100 ml quantity at 10 ppm and the effective decoloration is taken as a control. The degrading rate of malachite green endures with the presence of high polysaccharides and low protein content in the applied concentration of plant sources. Initially, from lower to 5% concentration of plant, the decoloration percentage raises and lowers at higher concentration due to the onset coloration of yellowish seed extract.

The photodegradation test was conducted by transferring the essential quantity of $CeO_2$ and $Mn:CeO_2$ nano-powders into a 50-ml beaker holding 30 ml of dye solution. To examine the photocatalytic activity, the experiments were steered for 60 min in UV light source, by effectively varying dye concentration (10–50 ppm), photocatalyst dosage (0.005–0.025 g), and pH of the dye solution (4–12). Initially, the combination of catalyst and dye solutions was stirred in the dark condition for 30 min to attain the whole adsorption equilibrium of the organic dyes by the catalyst. The blend solution was centrifuged to remove the catalyst and then 5 ml aliquots were exposed to light for every 10 min. After irradiation, the solution was shifted to the cuvette and the decolorization efficiency was intended from the diminution of absorbance noted in a spectrophotometer using wavelength 617 as a filter. To predict the dye elimination at high efficiency, the parameter like the amount of photocatalyst, concentration of dye, and pH of the solution was optimized. The efficient removal of malachite green has resulted in the

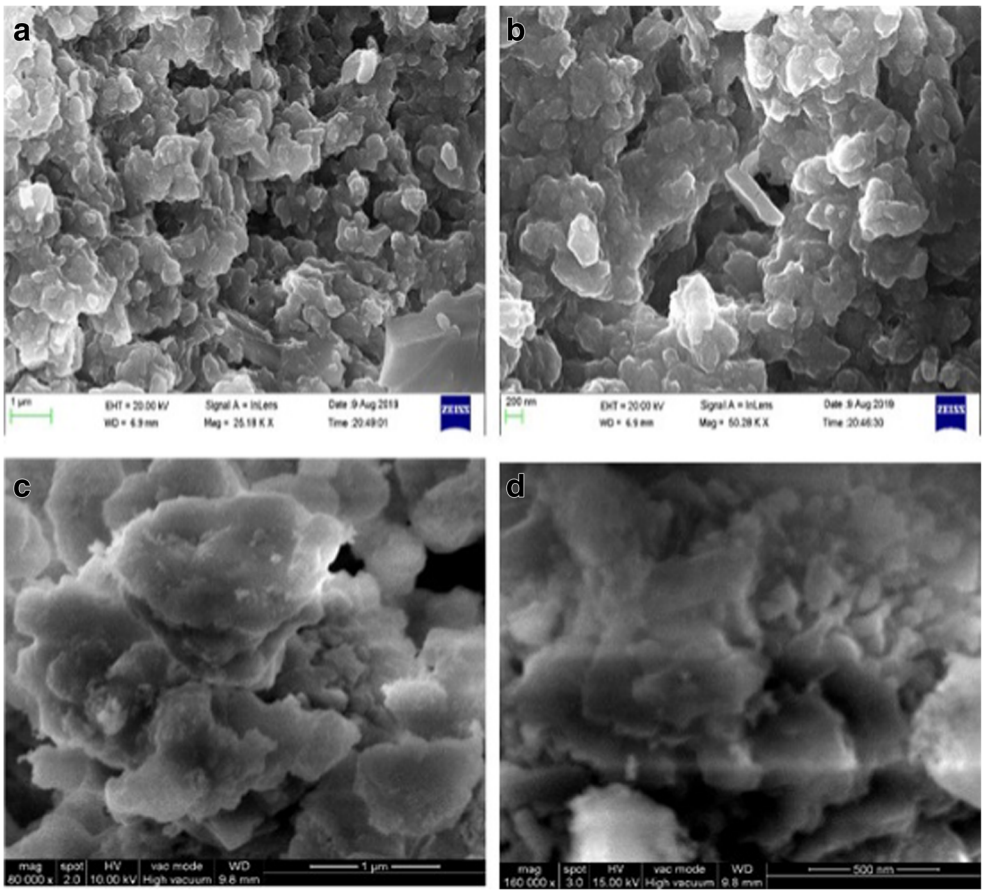


**Fig. 3** **a**, **b** FESEM images of $CeO_2$. **c**, **d** FESEM images of Mn:$CeO_2$ (CM2).

Mn:$CeO_2$ due to its condensed band gap compared with $CeO_2$ and it simplifies the formation of charge carriers by the UV radiation source. The kinetics work was determined by using the optimized parameter for $CeO_2$ and Mn:$CeO_2$ nano-powders. This practice was triplicated for each photocatalysis trials and the percentage degradation of MG was assessed using the following equation:

$$\%\textbf{Dye degradation} = (\mathbf{C_o} - \mathbf{C_t})/\mathbf{C_o} \times \mathbf{100}$$

## Result and discussion

### Mechanism of green synthesis

The formation of $CeO_2$ NPs revealed the occurrence of a schematic reaction by ammonium ceric sulfate with aqueous *Cassia angustifolia* seed extract. The yellow-colored phyto-mediated $Ce^{4+}$ complex solution was designed by the contact of phytochemicals in seed extract with cerium ions resulting in a harmonious effect. After washing the impurities, the sample was dried in a domestic micro-oven and the complexed sample suffered slow and generated stable pure $CeO_2$ nanoparticles. To prepare Mn:$CeO_2$, the substitution tactic was used along with seed extract. The lower oxidation state metal ion ($Mn^{2+}$) was supplemented on the nano-cerium oxide structure through accumulating dissimilar concentration of Mn contents and coded as CM1 (2.5 mol% ratio = 0.62% of Mn precursor in 99.38% Ce precursor), CM2 (5.0 mol% ratio = 1.387% of Mn precursor in 98.613% Ce precursor), and CM3 (7.5 mol% ratio = 1.98% of Mn precursor in 98.02% Ce precursor). The mixtures were momentously boosted by stirring and the precipitated complex was washed, and well dried in a micro-oven. The coloration of resultant samples gets varied on unlike attentiveness of Mn ions decorated on $CeO_2$ and the characterization gives the wide-ranging optical properties, crystalline morphology, and size. The oxygen vacancies in the samples (CM1, CM2, CM3) get regulated and the dye-degrading nature significantly improved the catalytic activities of $CeO_2$ (Slostowski et al. 2013).

### UV–visible diffuse reflectance spectroscopy

The UV–vis DRS was used to investigate the optical properties and their results were shown in Fig. 1. Some disorders may appear in the $CeO_2$ due to higher oxygen vacancies due to calcination and it was not preferred in all the samples. The

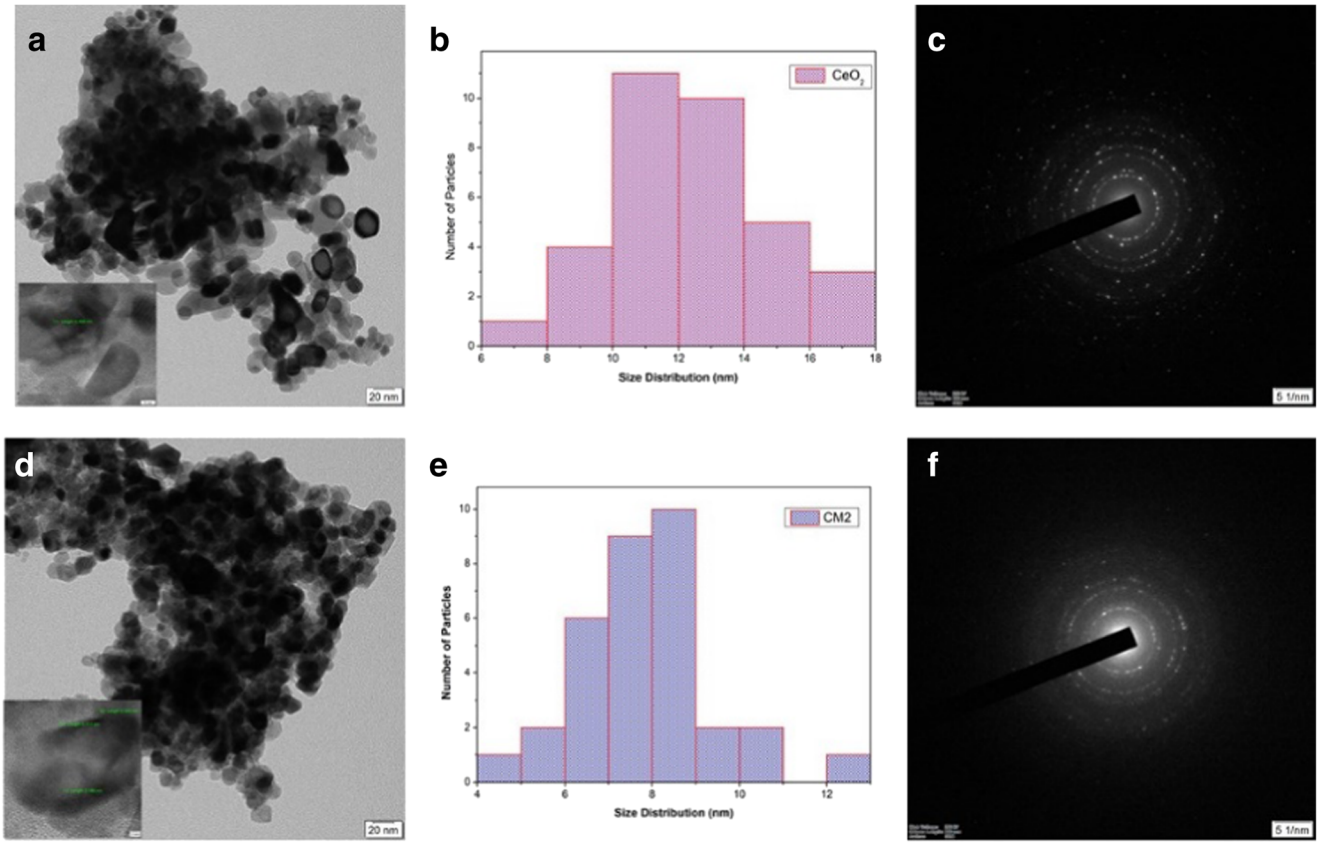


**Fig. 4** **a**, **d** HRTEM images of $CeO_2$ and CM2, and inset images denote the nanoparticles at lower magnification. **b**, **e** Histogram of $CeO_2$ and CM2. **c**, **f** SAED images of $CeO_2$ and CM2.

energy band plays a vital role in defining the photocatalytic activities of the semiconductor (Adepu et al. 2017). Figure 1a displays the UV–vis absorption spectrum of all samples, in the range of 200–800 nm and the samples exhibit strong absorption peaks in 365, 368, 378, and 367 nm. Figure 1b shows the percentage of reflectance of all the samples.

The optical absorption regularly obeys the Kubelka-Munk equation: $(F(r)\,h\nu)^{1/n} = A\,(h\nu - E_g)$, where $A$ is a constant, $h\nu$ is the photon energy, $E_g$ is the band gap, and F(r) is the absorption coefficient. Figure 1c portrays a Tauc plot from which the band gap energy ($E_g$) was determined for all the samples. The $E_g$ value is assessed at zero absorption as the intersection of the extrapolating linear portion with the $x$ axis. The $E_g$ value of the prepared samples was found to be 3.96 eV. This value is higher than those reported previously by Ramadoss and Kim (2012) and Truffault et al. (2010). Band gap for pure $CeO_2$ is 3.401 eV, 2.5 mol% (CM1) is 3.369 eV, 5 mol% (CM2) is 3.279 eV, and 7.5 mol% (CM3) is 3.375 eV. CM2 shows the highest absorption coefficient and then decreases on increasing the Mn concentration due to extra electronic energy levels inside the band gap, which will effectively narrow the band gap and increase the crystalline size (Yue and Zhang 2009; Atif et al. 2019).

## XRD pattern

In Fig. 2 a, all the observed peaks for pure $CeO_2$ were well indexed to cerium oxide ($CeO_2$) with a cubic fluorite structure (JCPDS card no. 34–0394). The observed peaks of Mn:$CeO_2$ (CM1, CM2, CM3) were found to be in the cubic fluorite structure. For $CeO_s$, the peak is narrow and becomes broad with low intensity due to the presence of decorated material Mn on $CeO_2$. XRD pattern confirmed that the decorated Mn has occupied the lattice positions in the crystal structure of $CeO_2$ nanoparticles.

On further increase in Mn concentration, Mn ions lose the capacity to enter the lattice site of $CeO_2$ and so it reduces the risk of increasing crystallite size (Khade et al. 2016). To predict the crystallite size, the strongest diffraction peak (111) is chosen for all the samples and the outcome of different mole percent of Mn on $CeO_2$ was assessed by Scherrer's equation, $D = K\lambda/\beta\cos\theta$, where $K$ is the constant (liable to half altitude width of nominated diffraction peak—0.9), $\lambda$ is the wavelength of X-ray (0.15418 nm), $\beta$ is the half-height width, and $\theta$ is the Bragg angle. The crystal size was starting to vary with different Mn concentrations which were fixed by broadening of the peaks. The crystalline size of pure $CeO_2$ is 14.17 nm and Mn:$CeO_2$ is (CM1) 12.06 nm, (CM2)

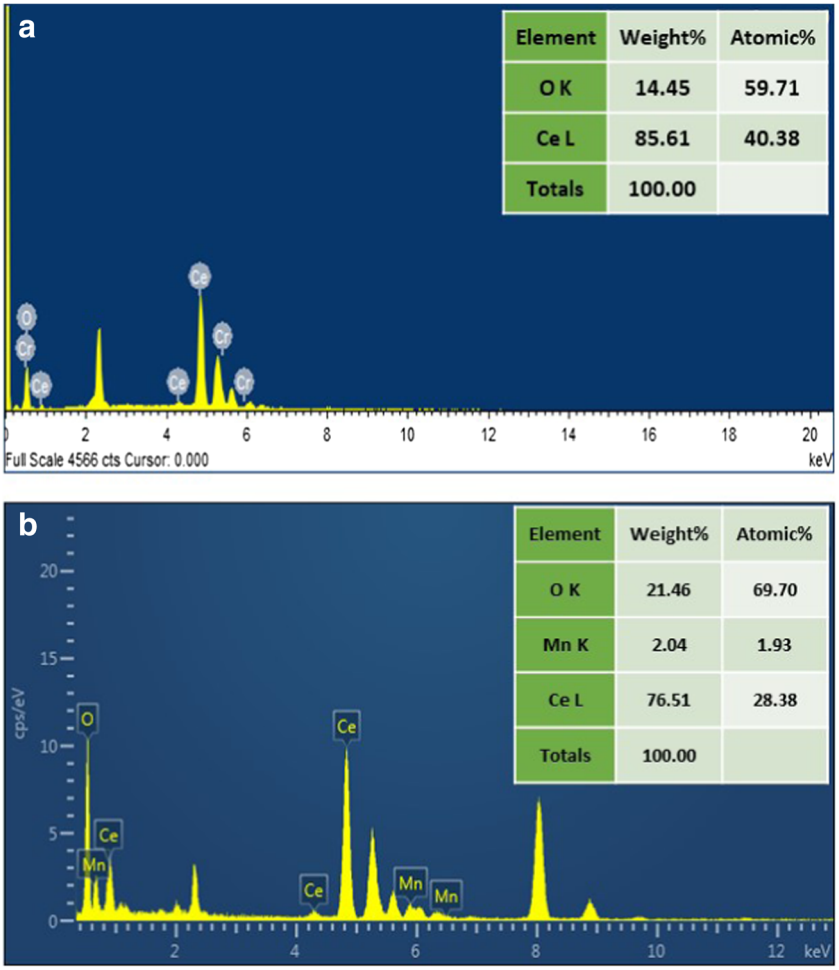


**Fig. 5** **a**, **b** EDAX of $CeO_2$ and CM2. Inset column predict the weight and atomic percent.

9.69 nm, and (CM3) 15.08 nm with (111) peak positioning at 2θ which were 28.03, 26.21, 26.4, and 26.36 and peak broadening $\beta = 0.58$, 0.67, 0.88, and 0.82. By fluctuating the Mn concentration more in 2.5 mol% and 5 mol%, the crystallite size gets shrink and secure by an expansion of the peaks. When the Mn concentration is greater than 5 mol%, the formation of clusters might occur largely which leads to size increment. Hence, in our work, we selected 5% Mn loading as an extreme concentration, to lean towards size lessening for defect formation in the $CeO_2$ lattice owed to Mn ions. So, it can be inferred that the decrease in crystallite size with 2.5 mol% and 5 mol% results in high firmness in the crystal lattice strain (Saranya et al. 2014). So, it is evident that the decrease in crystallite size with an increase in Mn concentration and the surface area of the samples can change the physical property, reactivity, and photochemical efficiency (Kumar et al. 2012). Further, increment of Mn content favored sintering and loss of intra-particle porosity, which was detrimental to the photocatalytic efficiency. The tuned band gap and smallest crystalline size of 5 mol% Mn-decorated $CeO_2$ were chosen for further characterization and photocatalytic degradation to compare with pure $CeO_2$.

## FT-IR analysis

Figure 2b displays the FTIR spectrum of plant, $CeO_2$, and Mn:$CeO_2$ (CM2) NPs. The functional group existing in the biomolecules of *Cassia angustifolia* seed extract display peaks at 878.42 $cm^{-1}$ (C–H), 1034.61 $cm^{-1}$ (C–O), 1403.93 $cm^{-1}$ (C=C), 1563.91 $cm^{-1}$ (N–H), and 3281 $cm^{-1}$ (O–H). For pure $CeO_2$, the absorption band located at 539.971 $cm^{-1}$ is assigned to the stretching vibration of the Ce–O bond (Athawale et al. 2009). The band positioned in 1044.26 $cm^{-1}$ is ascribed to C–O stretching vibration (Murugana et al. 2018) in $CeO_2$. The band placed at 1629.55 and 1428.99 $cm^{-1}$ is attributed to N–H and C–H bending vibration (Prabaharan et al. 2016) present in $CeO_2$. The weak band detected at 2106.85 $cm^{-1}$ is allotted to C–H stretching vibration, and this indicates the presence of organic compounds gets adsorbed onto the surface of pure $CeO_2$ (Athawale et al. 2009). The broad bands sited at 3223.43 and 1052.94 $cm^{-1}$ are credited to stretching and bending vibrations of the O–H group attached to nano-$CeO_2$. For Mn:$CeO_2$, the appearance of broad bands around 593.97 and 481.153 $cm^{-1}$ is allotted

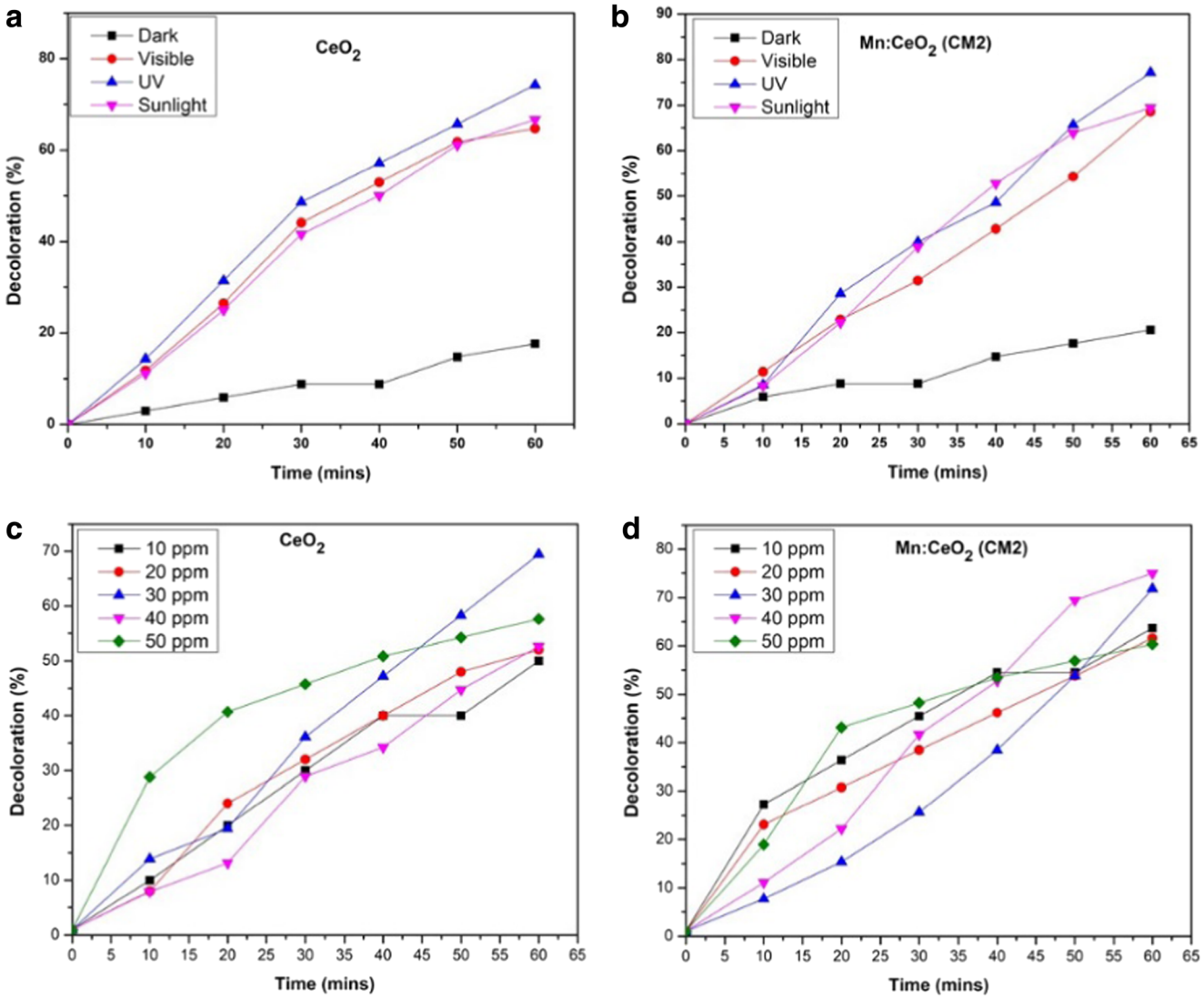


**Fig. 6** **a**, **b** Decoloration percentage of MG at different light sources for $CeO_2$ and Mn:$CeO_2$ (CM2). **c**, **d** Decoloration percentage of MG at different dye concentrations for $CeO_2$ and Mn:$CeO_2$ (CM2).

to the Ce–O–Ce and Ce–O–Mn vibrational symmetrical stretching frequencies (Ho et al. 2005). The band is observed at 1044 $cm^{-1}$ owing to the alteration of longer Ce = O group in the nanostructure (Binet et al. 1994). Mostly, the addition of Mn ion in $CeO_2$ outcomes in a descending swing of photosensitive mode and peak changes to higher frequency 3241.75 $cm^{-1}$ (O–H), 1631.48 $cm^{-1}$ (N–H), and 2280.41 $cm^{-1}$ (C–H) stretching, when interrelated to pure $CeO_2$. The shift in the peak of Mn:$CeO_2$ and changes in the length of oxygen bond in $CeO_2$ were due to the implementation of Mn ions in the $CeO_2$ lattice.

## Investigation on stability

Zeta potential was predicted with charges based on the potential difference and discrete solvent has an opposite charge on the surface of the nanoparticles. Figure 2c displays the zeta potential value of synthesized $CeO_2$ and Mn:$CeO_2$ as −43.1 mV and − 33.2 mV with particle size 27.9 nm and 25.4 nm SD. Mostly, zeta potential with higher negative value specifies extra disgust among the particles which diminishes aggregation for high stable NPs (Nezhad et al. 2020). The exceeded negative charge retorts the stability and proves the surface of nanoparticles was adorned with phyto molecules of *Cassia angustifolia* seed.

## FESEM, HRTEM, and EDAX analysis

The morphology of green fabricated pure $CeO_2$ and Mn:$CeO_2$(CM2) surfaces was investigated using a field emission scanning electron microscope (FESEM) and the results were shown in Fig. 3a, b, c, and d. The surface morphology of

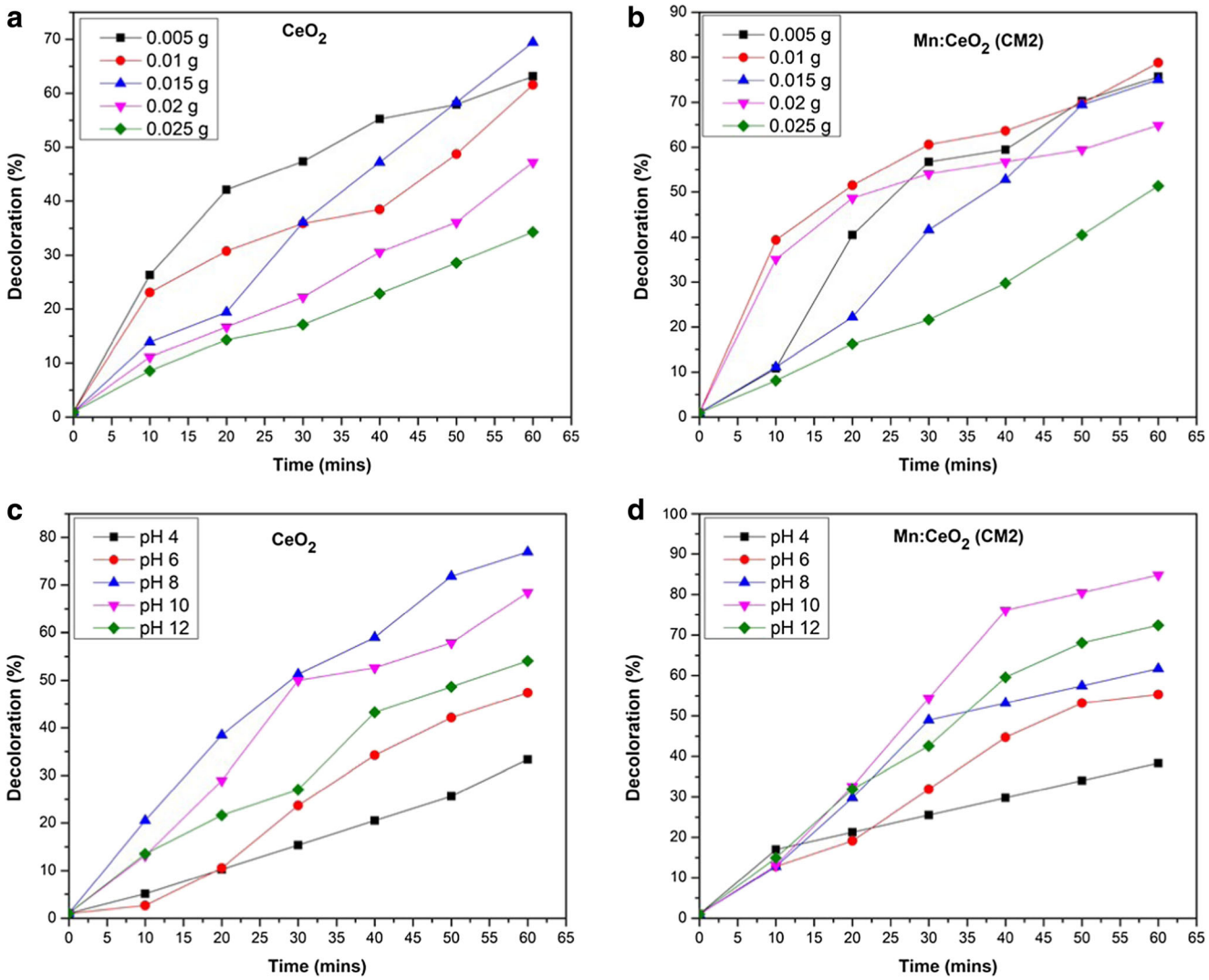


**Fig. 7** **a**, **b** Decoloration percentage of MG at different amount of photocatalyst loaded for $CeO_2$ and Mn:$CeO_2$ (CM2). **c**, **d** Decoloration percentage of MG at different pH for $CeO_2$ and Mn:$CeO_2$ (CM2).

pure $CeO_2$ was measured in 1 μm and 200 nm scales and Mn:$CeO_2$ measured in 1 μm and 500 nm scales which is agglomerated as uneven particles due to highly stable and permitting crystal growth (Choi et al. 2016). The micro and nano-morphology of pure $CeO_2$ gather like spherical. On Mn:$CeO_2$, extreme transformation in shape was detected as flower-like morphology due to augmentations of metal nucleation cores and favored positioning peak deviations in the X-ray diffraction pattern (Yanan et al. 2013).

The HRTEM images, histogram, and SAED image of pure $CeO_2$ and Mn:$CeO_2$ (CM2) are shown in Fig. 4. In HRTEM, the size of the $CeO_2$ and Mn:$CeO_2$ (CM2) nanoparticle was calculated using the Digimizer Image Analysis software as 10–12 nm and 8–9 nm. The HRTEM images revealed that the average particle size 11 nm for pure $CeO_2$ and 9 nm for CM2 was given in Fig. 4(a, d) and the inset figure shows its lower magnification. The inset figure of $CeO_2$ and Mn:$CeO_2$ explains the variation occurs in the inter-planer distance. Histogram explains the size distribution for a different count of particles exhibits maximum in the range 10–12 nm for pure $CeO_2$ and 8–9 nm for CM2 which was shown in Fig. 4(b, e). The consequences elucidate the reduction in average particle size Ce(IV) by additional optimized concentration of Mn(II) ions at CM2 (Saranya et al. 2014) and also due to the replacement of Ce(IV) with Mn(II) ions (Kumar et al. 2012). Fig. 4 c and f predict the SAED patterns attained by converging the beam on the $CeO_2$ and Mn:$CeO_2$ demonstrates the cubic single phase and purity.

The energy-dispersive X-ray spectra give qualitative and quantitative presence elements in pure $CeO_2$ and Mn:$CeO_2$ (CM2). Fig. 5 a and b show the spectra of protruding peaks with dissimilar intensities corresponding to Ce and O for pure $CeO_2$ and Mn, Ce, and O for Mn:$CeO_2$. Inset images predict the clear appearance of weight and atomic percentage.

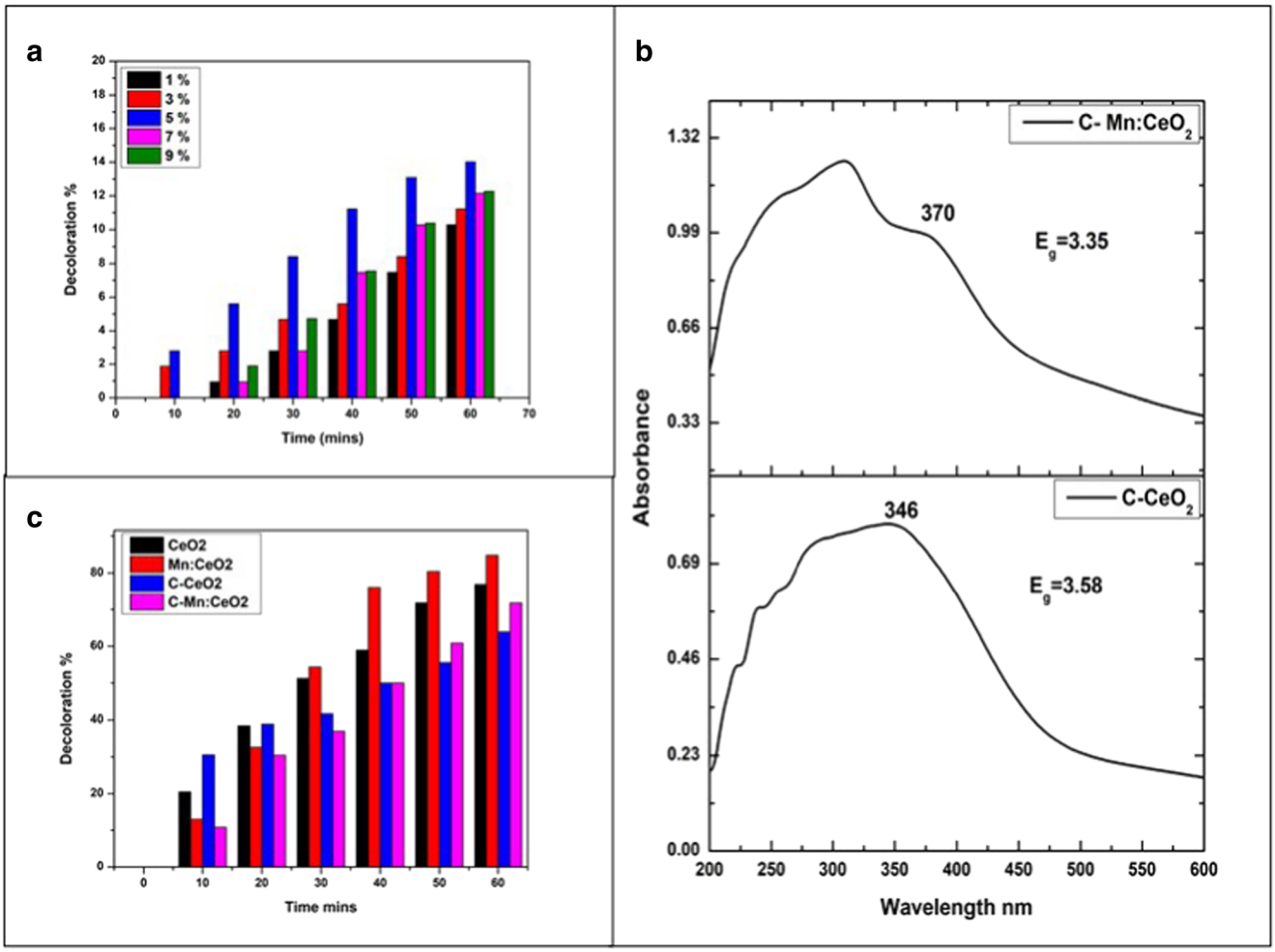


**Fig. 8** **a** Decoloration percentage with *Cassia angustifolia* seed. **b** UV-DRS of C-$CeO_2$ and C-Mn:$CeO_2$. **c** Decoloration percentage of conventional (C-$CeO_2$ and C-Mn:$CeO_2$), and green synthesis ($CeO_2$ and Mn:$CeO_2$)

## Photocatalytic activity of $CeO_2$ and Mn:$CeO_2$ (CM2)

### Setting optimum parameters in photodegradation

The high-efficient photodegradation was analyzed in $CeO_2$ and Mn:$CeO_2$ by varying light radiation, dye concentration, catalyst loading, and pH. The rate and efficiency of dye degradation vary with the respective time and the radiation of light. By capturing visible and UV sunlight, the valence electron in the catalyst moves to the excited state and it leads to the formation of photoelectron. In dark conditions, the same photocatalyst was applied on the dye and it is compared with the radiation condition. In Fig. 6(a, b), the results of dark and dissimilar light sources for $CeO_2$ and Mn:$CeO_2$ are compared and concluded in which UV light source holds good for the degradation process with respective reaction time. If the intensity of UV radiation is more than an hour, the active sites of the catalyst will get accumulated and create photocatalyst deactivation (Li et al. 2008). Though degradation increases with an increase in time, we preferred effective degradation in a short time (within 60 min). The optimized UV light radiation was emitted for 60 min by loading 0.02 g $CeO_2$ and Mn:$CeO_2$ catalyst to 30 ml of different concentrations of dye solutions (10 ppm, 20 ppm, 30 ppm, 40 ppm, and 50 ppm) with its pH 5.3. Fig. 6 c and d show the degradation efficiency of dyes at 30 ppm for $CeO_2$, and 40 ppm for Mn:$CeO_2$. The excess concentration of dye reduces the e−/h + recombination rate on formation of free oxygen $O_2^{\bullet}$ radicals and hydroxyl radical $OH^{\bullet}$ will never adsorb on the surface of the catalyst but stabilize intermediate radicals that is accountable for the mineralization of the dye molecule and it leads the way to pollute water (Fujishima et al. 2008).

The consequences of $CeO_2$ and Mn:$CeO_2$ photocatalyst were loaded in varying amounts (0.005 g, 0.01 g, 0.015 g, 0.02 g, and 0.025 g) on 30 ml of 30 ppm dye solution by irradiation time of 60 min at its pH 5.3. Fig. 7 a and b show the extreme degradation of 0.02 g for $CeO_2$ and 0.01 g for Mn:$CeO_2$, and a further increase in photocatalyst decreases the degradation rate. When the photocatalyst amount is more

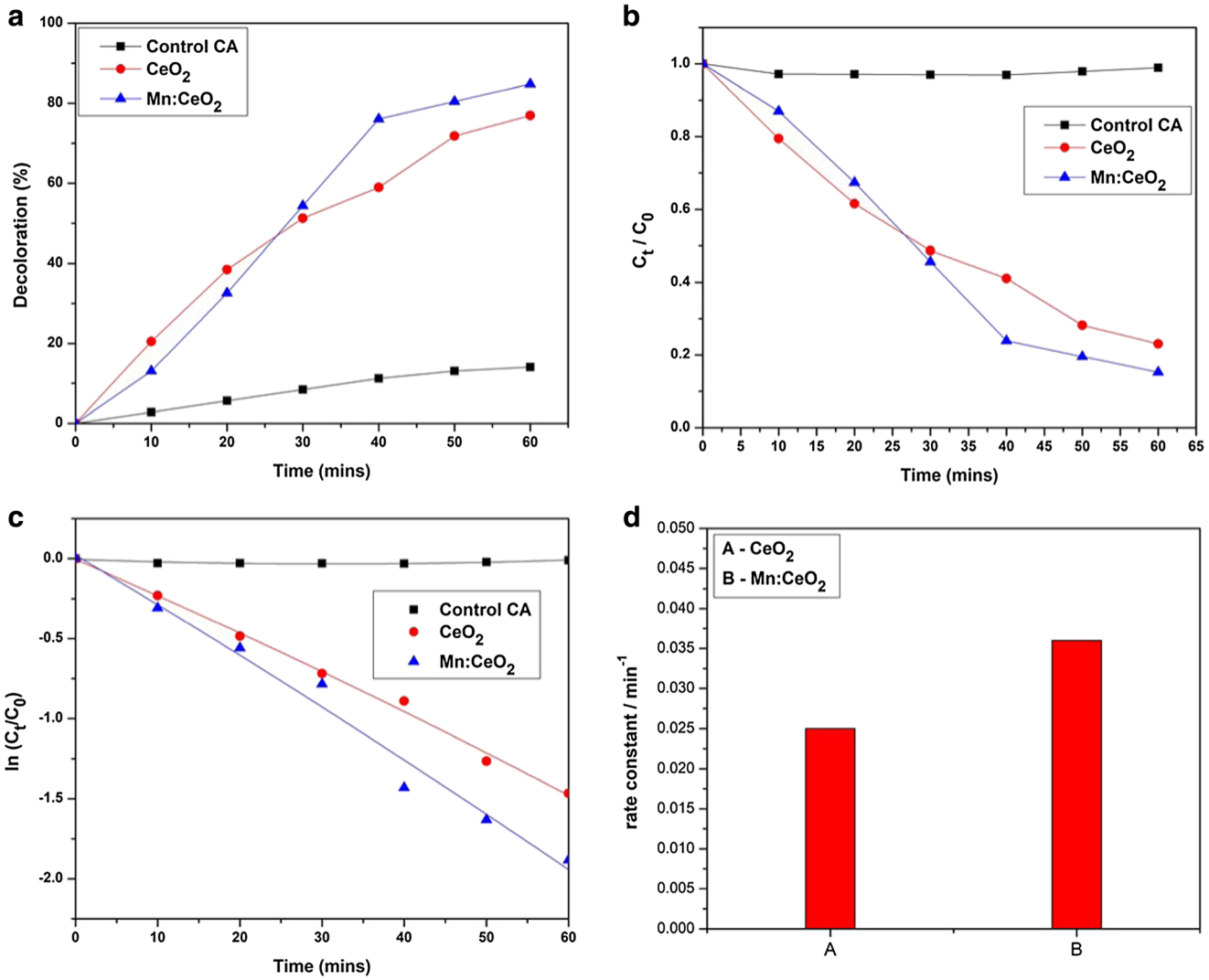


**Fig. 9** **a** Decoloration percentage of MG dye using $CeO_2$ and Mn:$CeO_2$. **b**, **c** Kinetic plots for MG degradation using $CeO_2$ and Mn:$CeO_2$. **d** Rate constant for $CeO_2$ and Mn:$CeO_2$

than an optimum level, the OH radical counts get more to cause dense solution which affects the activation of the catalyst by light, so the degradation rate is reduced (Sun et al. 2008). The adjustment of malachite green to different pH gets changed by adding a trace solution of diluted hydrochloric acid or sodium hydroxide to normal pH 5.3. The pH impacts on the surface state of the catalyst and ionization state of ionizable dye molecules. The amount of photodegradation gets affected by pH, it alters the charges on the surface of the catalyst, and it leads to protonation or deprotonation, and also it depends on the nature of the dye (Wang et al. 2012). The active •OH at high pH acts as the best oxidant and creates electrostatic attractive properties among the catalyst and the functioning dye molecules (Daneshvar et al. 2003). For distinct pH from 4 to 12, the decoloration efficiency was shown in Fig. 7(c, d) with 0.02 g of $CeO_2$ and Mn:$CeO_2$ photocatalysts applied in 30 ppm dye solutions. The decoloration efficiency confirms the pH value ascribed for $CeO_2$ is 8 and Mn:$CeO_2$ is 10. On applying the optimized parameters, the decoloration efficiency was noted for $CeO_2$ and Mn:$CeO_2$.

Just to compare the decoloration efficiency of green synthesized nanoparticles $CeO_2$ and Mn:$CeO_2$, we synthesized $CeO_2$ and Mn:$CeO_2$ conventional method using NaOH replacing the *Cassia angustifolia* seed extract. For the conventional synthesized samples, the band gap is noted from the UV-DRS wavelength and coded as C-$CeO_2$ and C-Mn:$CeO_2$ as shown in Fig. 8 b. The conventional nanomaterials were applied in malachite green with optimized parameters as used for the green synthesis decoloration part. Figure 8c displays the comparable resulted values of malachite green degradation with green synthesized and conventional nanoparticles. From the display, we can be able to note some extent progressive degradation consequence for green synthesized materials. The advanced result may arise owing to the small band gap and nano-textured size.

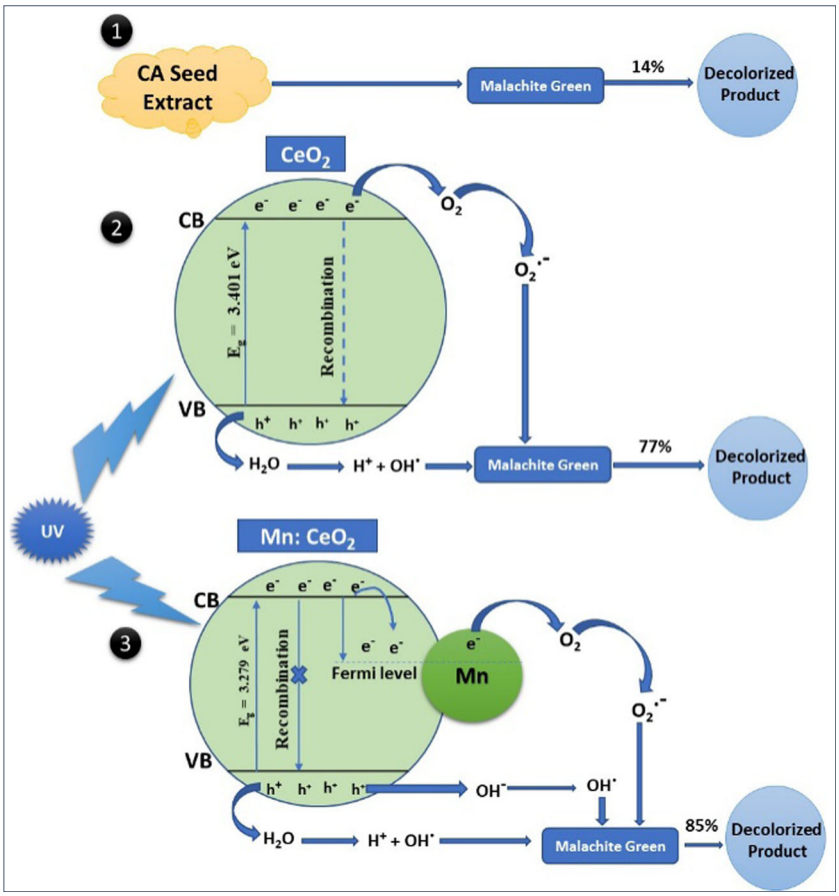


**Fig. 10** Photocatalytic mechanism

## Kinetics study of malachite green degradation

Experiments were made by using an optimized amount of dye concentration, $CeO_2$, and Mn:$CeO_2$ (CM2) photocatalyst loading, required pH, and light source for the 1-h time duration, and its decoloration efficiency was shown in Fig. 9a along with *Cassia angustifolia* seed. The result describes that the Mn-decorated $CeO_2$ at 5 mol% (CM2) is 3.279 eV which shows better results equated with pure $CeO_2$ 3.401 eV photocatalyst. The optimized conditions for decolorizing MG are analyzed with *Cassia angustifolia* seed, $CeO_2$, and Mn:$CeO_2$. The kinetics rate was planned only for efficient degradation with green synthesized $CeO_2$ and Mn:$CeO_2$. The degradation kinetics was predicted by the equation $(-\ln (C_t/C_0) = kt)$ where $k$ is the rate constant, and $C_t$ and $C_0$ are the concentrations of final time and initial time respectively (Behrouz et al. 2019).

The kinetics study in photocatalytic decoloration of malachite green by $CeO_2$ and Mn:$CeO_2$ and their plots of $-\ln (C_t/C_0)$ versus irradiation time gives straight line which were shown in Fig. 9c. Probably, kinetics depends on the dye charge and sensitive surface of synthesized nanoparticles. In the green nano-ZnO photocatalyst, degradation of Congo Red and Rose Bengal dye tracks a comparable kinetics model (Vidya et al. 2016, 2017). The first-order rate constants are given by the slope 0.0245 and 0.0327 $min^{-1}$ for $CeO_2$ and Mn:$CeO_2$ respectively. Hence, we suggest from our results that the surface of Mn:$CeO_2$ is more reactive in adsorption of dye molecules compared with $CeO_2$ due to the finest size and aggregation of flower-like morphology. We conclude that the probable Mn:$CeO_2$ photocatalyst appears to be hopeful in the degradation of contaminated dyes in water within a short time.

## Probable photocatalysis mechanism

Figure 10 explains the mechanism of decoloration using Cassia seed, green synthesized $CeO_2$, and Mn:$CeO_2$. The principle of photocatalysis was redox reaction which gets initiated by the interaction of drift charge carriers generated on the surface of the photocatalyst to adsorb the dye molecules (Tachikawa et al. 2007).

Dye removal undergoes numerous oxidative paths depending on the size and surface of the photocatalyst as follows:

- Formation of oxidizing hydroxyl free radicals (•OH) by holes (+) in the valence band (VB) intermingles with $H_2O$ and OH group on the surface of the catalyst.

- Development of superoxide ion ($O_2^{\cdot-}$) by electrons (−) in the conduction band (CB) with oxygen molecules exists on the nano-catalyst surface.
- Abundant rise of surface hydroxyl radical in Mn:$CeO_2$ was due to the presence of accurate Mn ion on $CeO_2$ lattice, ability to capture the light-induced electron and transfer to oxygen present on the surface of $CeO_2$.
- All these radicals combine to give effective decoloration of MG.

## Conclusion

In swift, facile green nanofabrication of $CeO_2$ and Mn:$CeO_2$ was prepared using phytochemicals of *Cassia angustifolia* seed extract. The green synthesis predicts smaller nanoparticles and it was noted through HRTEM. Since the weak base occurs in *Cassia angustifolia* seed extract, the formation of nanoparticles takes place for a longer duration with low temperature. Thus, the resultant nanoparticle holds good stability and capped with phyto molecules. The FT-IR of nano-$CeO_2$ exhibits the presence of *Cassia angustifolia* phyto groups (–OH, –CH, –NH) on its surface. In XRD, less intense peak was obtained compared with chemical synthesis, but no extra peak was detected. From our result, the green synthesized $CeO_2$ exists in a pure and stable form. Similar to pure $CeO_2$, the green nano-Mn:$CeO_2$ also exists in stable form, on characterizing and applying the synthesized samples along with *Cassia angustifolia* seed and conventionally prepared C-$CeO_2$ and C-Mn:$CeO_2$ nanomaterials. Among all decoloration efficiency, green synthesized pure nano-$CeO_2$ and Mn:$CeO_2$ (CM2) under the optimal conditions were attained by changing radiation including dark, concentration of MG, catalyst dosage, and pH of dye solution. The reaction kinetics was effectively supervised by spectrophotometer readings, and the kinetics process was well projected to the first-order model. The extreme efficiency of MG degradation was achieved in short duration by Mn:$CeO_2$ (CM2) photocatalyst under UV radiation to degrade universal water pollutant malachite green.

**Acknowledgments** We thank Madras Christian College, Chennai, Tamil Nadu, for providing the necessary facilities. We gratefully acknowledge our principal Dr. P. Wilson and Head of Chemistry Department Dr. E. Iyyappan for their support. We thank SRM University for the XRD, SEM, and HRTEM measurements.

**Authors' contributions** All the authors have contributed to the structural formation of this work. A. Dhivya has performed the experimental part and data analysis and interpreted the data. The manuscript was checked and corrected by Dr. Rakhi Yadav. Finally, all the authors have read and approved the submitted manuscript and authors' responses to the reviewer's comments to the *Environmental Science and Pollution Research* journal.

**Data availability** The datasets used and analyzed during the current study are available from the corresponding author on reasonable request.

## Compliance with ethical standards

**Conflict of interest** The authors declare that they have no conflict of interest.

**Ethical approval and consent to participate** Not applicable.

**Consent to publish** Not applicable.

## References

Adepu Ak, Katta V, Venkatathri N (2017) Synthesis, characterization, and photocatalytic degradation of Rhodamine B dye under sunlight irradiation of porous titanosilicate (TS)/bismuth vanadate ($BiVO_4$) nanocomposite hybrid catalyst. New J Chem 41:2498. https://doi.org/10.1039/C7NJ00071E

Athawale AA, Bapat MS, Desai PA (2009) Hydroxide directed routes to synthesize nanosized cubic ceria ($CeO_2$). J Alloys Compd 484:211. https://doi.org/10.1016/j.jallcom.2009.03.125

Atif M, Iqbal S, Fakhar-E-Alam M, Qaisar Mansoor IM, Mughal L, Aziz MH, Hanif A, Farooq WA (2019) Manganese-doped cerium oxide nanocomposite induced photodynamic therapy in MCF-7 cancer cells and antibacterial activity. BioMed Research International, Article ID 7156828:13. https://doi.org/10.1155/2019/7156828

Behrouz E, Mirzaee M, Darroudi M, Oskuee RK, Sadri K, SadeghAmiri M (2019) Preparation of cerium oxide nanoparticles in Salvia macrosiphon Boiss seeds extract and investigation of their photocatalytic activities. Ceram Int 45(4):4790–4797. https://doi.org/10.1016/j.ceramint.2018.11.173

Binet C, Badri A, Lavalley JC (1994) A spectroscopic characterization of the reduction of ceria from electronic transitions of intrinsic point defects. J Phys Chem 98:6392–6398. https://doi.org/10.1021/j100076a025

Bodaiah B, Bhushanam K, Konduri VV, Mangamuri UK, Gorrepati R, Poda S (2018) Green synthesis of silver and gold nanoparticles using Stemona tuberosa Lour and screening for their catalytic activity in the degradation of toxic chemicals. Environ Sci Pollut Res. https://doi.org/10.1007/s11356-018-3105-9

Choi J, Amaranatha Reddy D, Jahurul Islam M, Ma R, Kim TK (2016) Self-assembly of $CeO_2$ nanostructures/reduced graphene oxide composite aerogels for efficient photocatalytic degradation of organic pollutants in water, journal of alloys and compounds, volume 688, part B. Pages 527-536. https://doi.org/10.1016/j.jallcom.2016.07.236

Daneshvar N, Salari D, Khataee AR (2003) Photocatalytic degradation of azo dye acid red 14 in water: investigation of the effect of operational parameters. J Photochem Photobiol A Chem 157:111–116. https://doi.org/10.1016/S1010-6030(03)00015-7

Dhivya A, Yadav R, Pandian K (2020) Enhanced antimicrobial and cytotoxicity on cancer cell using bio-originated selenium nanoparticles. Asian J Chem 32:543–549. https://doi.org/10.14233/ajchem.2020.22420

Feizpoor S, Habibi-Yangjeh A, Yubuta K, Vadivel S (2019) Fabrication of TiO2/CoMoO4/PANI nanocomposites with enhanced photocatalytic performances for removal of organic and inorganic pollutants under visible light. Mater Chem Phys 224:10–21. https://doi.org/10.1016/j.matchemphys.2018.11.076

Fujishima A, Zhang X, Tryk DA (2008) $TiO_2$ photocatalysis, and related surfacephenomena. Surf Sci Rep 63:515–582. https://doi.org/10.1016/j.surfrep.2008.10.001

Gnanam S, Rajendran V (2018) Facile sol-gel preparation of cd-doped cerium oxide ($CeO_2$) nanoparticles and their photocatalytic activities. J Alloys Compd 735:1854. https://doi.org/10.1016/j.jallcom.2017.11.330

Goubin F, Rocquefelte X, Whangbo MH, Montardi Y, Brec R, Jobic S (2004) Experimental and theoretical characterization of the optical properties of $CeO_2$, $SrCeO_3$, and $Sr_2CeO_4$ containing Ce4+ (f0) ions. Chem Mater 16:662–669. https://doi.org/10.1021/cm034618u

Herrling T, Seifert M, Jung K (2013) Cerium dioxide: future UV-filter in sunscreen. SOFW J 139:12

Higashimoto S, Tanaka Y, Ishikawa R, Hasegawa S, Azuma M, Ohue H, Sakata Y (2013) Selective dehydrogenation of aromatic alcohols photocatalyzed by Pd-deposited CdS–$TiO_2$ in aqueous solution using visible light. Catal Sci Technol 3:400. https://doi.org/10.1039/C2CY20607B

Ho C, Yu JC, Kwong T, Mak AC, Lai S (2005) Morphology-controllable synthesis of mesoporous CeO2 nano- and microstructures. Chem Mater 17:4514–4522. https://doi.org/10.1021/cm0507967

Khade GV, Suwarnkar MB, Gavade NL, Garadkar KM (2016) Sol-gel microwave assisted synthesis of Sm-doped $TiO_2$ nanoparticles and their photocatalytic activity for the degradation of methyl Orange under sunlight. J Mater Sci Mater Electron 27:6425–6432. https://doi.org/10.1007/s10854-016-4581-7

Kumar CHSSP, Balaguru RJB, Jeyaprakash BG (2012) Influence of Mn doping on physical properties of nanostructured $CeO_2$ thin films. J Appl Sci 12:1738–1741. https://doi.org/10.3923/jas.2012.1738.1741

Li R, Yabe S, Yamashita M, Momose S, Yoshida S, Yin S, Sato T (2002) Synthesis and UV-shielding properties of ZnO- and CaO-doped $CeO_2$ via soft solution chemical process. Solid State Ionics 151:235–241. https://doi.org/10.1016/S0167-2738(02)00715-4

Li Y, Sun S, Ma M, Ouyang Y, Yan W (2008), Kinetic study and model of the photocatalytic degradation of rhodamine B (RhB) by a $TiO_2$-coated activated carbon catalyst: effects of initial RhB content, light intensity and $TiO_2$ content in the catalyst, Chemical Engineering Journal, Volume 142, Issue 2, 15 August 2008, Pages 147–155, https://doi.org/10.1016/j.cej.2008.01.009

Li H, Wang G, Zhang F, Cai Y, Wang Y, Djerdj I (2012) Surfactant-assisted synthesis of $CeO_2$ nanoparticles and their application in wastewater treatment. RSC Adv 2:12413–12423. https://doi.org/10.1039/C2RA21590J

Lu XW, Li XZ, Qian JC, Miao NW, Yao C, Chen ZG (2016) Synthesis and characterization of $CeO_2$/$TiO_2$ nanotube arrays and enhanced photocatalytic oxidative desulfurization performance. J Alloys Compd 661:363–371. https://doi.org/10.1016/j.jallcom.2015.11.148

Manjoosha S, Srivastava S, Rawat AKS (2010) Chemical standardization of Cassia angustifolia Vahl seed. Phcog J 2(13):554–560. https://doi.org/10.1016/S0975-3575(10)80059-8

Mao C, Zhao Y, Qiu X, Zhu J, Burda C (2008) Synthesis, characterization, and computational study of nitrogen-doped $CeO_2$ nanoparticles with visible-light activity. Phys Chem Chem Phys 10(36):5633–5638. https://doi.org/10.1039/B805915B

Mohamed A, Ghobara MM, Abdelmaksoud MK, Mohamed GG (2019) A novel and highly efficient photocatalytic degradation of malachite green dye via surface modified polyacrylonitrile nanofibers/biogenic silica composite nanofibers. Sep Purif Technol 210:935–942. https://doi.org/10.1016/j.seppur.2018.09.014

Montini T, Melchionna M, Monai M, Fornasiero P (2016) Fundamentals and catalytic applications of $CeO_2$-based materials. Chem Rev 116:5987. https://doi.org/10.1021/acs.chemrev.5b00603

Murugan B, Ramaswamy AV, Srinivas D, Gopinath CS, Ramaswamy V (2005) Nature of manganese species in Ce1-xMnx$O_2$-d solid solutions synthesized by the solution combustion route. Chem Mater 17(15):3983–3993. https://doi.org/10.1021/cm050401j

Murugana R, Kashinath L, Subash R, Sakthivel P, Byrappa K, Rajendran S, Ravi G (2018) Pure and alkaline metal ion (mg, Ca, Sr, Ba) doped cerium oxide nanostructures for photo degradation of methylene blue. Mater Res Bull 97:319–325. https://doi.org/10.1016/j.materresbull.2017.09.026

Nagajyothi PC, Prabhakar Vattikuti SV, Devarayapalli KC, Yoo K, Shim J, Sreekanth TVM (2019) Green synthesis: photocatalytic degradation of textile dyes using metal and metal oxide nanoparticles-latest trends and advancements. Crit Rev Environ Sci Technol. https://doi.org/10.1080/10643389.2019.1705103

Nezhad SA, Es-haghi A, Tabrizi MH (2020) Green synthesis of cerium oxide nanoparticle using Origanum majorana L. leaf extract, its characterization, and biological activities. Appl Organomet Chem 34:e5314. https://doi.org/10.1002/aoc.5314

Pavan Kumar CHSS, Pandeeswari R, Jeyaprakash BG (2014) Structural, morphological and optical properties of spay deposited Mn-doped $CeO_2$ thin films. J Alloys Compd 602:180–186. https://doi.org/10.1016/j.jallcom.2014.02.143

Pavasupree S, Suzuki Y, Pivsa-Art S, Yoshikawa S (2005), Preparation and characterization of mesoporous $TiO_2$-$CeO_2$ nanopowders respond to visible wavelength;178(1):128–134. https://doi.org/10.1016/j.jssc.2004.10.028

Prabaharan DM, Sadaiyandi K, Mahendran M, Sagadevan S (2016) Structural, optical, morphological and dielectric properties of cerium oxide nanoparticles. Mat Res 19:478. https://doi.org/10.1590/1980-5373-MR-2015-0698

Prabaharan DM, Sadaiyandi K, Mahendran M, Sagadevan S (2018) Investigating the effect of Mn-doped $CeO_2$ nanoparticles by coprecipitation method. Applied Physics A 124(2):86. https://doi.org/10.1007/s00339-017-1518-9

Ramadoss A, Kim SJ (2012) Synthesis and characterization of $HfO_2$ nanoparticles by sonochemical approach. J Alloys Compd 544:115. https://doi.org/10.1016/j.jallcom.2012.08.005

Rashmi S, Bhatttacharya B, Singh V (2002) *Cassia angustifolia* seed gum as an effective natural coagulant for decolourisation of dye solutions. Green Chem 4:252–254. https://doi.org/10.1039/b200067a

Saranya J, Ranjith KS, Saravanan P, Mangalaraj D, Rajendra Kumar RT (2014) Cobalt-doped cerium oxide nanoparticles: enhanced photocatalytic activity under UV and visible light irradiation. Mater Sci Semicond Process 26:218. https://doi.org/10.1016/j.mssp.2014.03.054

Shabina IA, Hayat MQ, Tahir M, Mansoor Q, Ismail M, Keck K, Bates RB (2016) Pharmacologically active flavonoids from the anticancer, antioxidant and antimicrobial extracts of Cassia angustifolia Vahl. BMC Complement Altern Med 16(460):1–9. https://doi.org/10.1186/s12906-016-1443-z

Sijo F, Joseph S, Koshy EP, Mathew B (2017) Green synthesis and characterization of gold and silver nanoparticles using *Mussaenda glabrata* leaf extract and their environmental applications to dye degradation. Environ Sci Pollut Res. https://doi.org/10.1007/s11356-017-9329-2

Slostowski C, Marre S, Bassata JM, Aymonier C (2013) Synthesis of cerium oxide-based nanostructures in near- and supercritical fluids. J Supercrit Fluids 84:89–97. https://doi.org/10.1016/j.supflu.2013.09.014

Sun J, Qiao L, Sun S, Wang G (2008) Photocatalytic degradation of Orange G on nitrogen-doped $TiO_2$ catalysts under visible light and sunlight irradiation. J Hazard Mater 155:312–319. https://doi.org/10.1016/j.jhazmat.2007.11.062

Tachikawa T, Fujitsuka M, Majima T (2007) Mechanistic insight into the $TiO_2$ photocatalytic reactions: design of new photocatalysts. J Phys Chem C 111:5259–5275. https://doi.org/10.1021/jp069005u

Tanur S, Ahmaruzzaman M (2015) Green synthesis of copper nanoparticles for the efficient removal (degradation) of dye from aqueous

phase. Environ Sci Pollut Res. https://doi.org/10.1007/s11356-015-5223-y

Truffault L, Ta MT, Devers T, Konstantinov K, Harel V, Simmonard C, Andreazza C, Nevirkovets IP, Pineau A, Veron O, Blondeau JP (2010) Application of nanostructured Ca doped $CeO_2$ for ultraviolet filtration. Mater Res Bull 45:527–535. https://doi.org/10.1016/j.materresbull.2010.02.008

Van Dao D, Nguyen TTD, Majhi SM, Adilbish G, Lee HJ, Yu YT, Lee IH (2019) Ionic liquid-supported synthesis of $CeO_2$ nanoparticles and its enhanced ethanol gas sensing properties. Mater Chem Phys 231:1–8. https://doi.org/10.1016/j.matchemphys.2019.03.025

Vidya C, Chandra Prabhab MN, Antony Raja MAL (2016) Green mediated synthesis of zinc oxide nanoparticles for the photocatalytic degradation of rose Bengal dye. Environmental Nanotechnology, Monitoring & Management 6:134–138. https://doi.org/10.1016/j.enmm.2016.09.004

Vidya C, Manjunatha. C, Chandraprabha. M.N, Megha Rajshekar, Antony Raj.M.A.L (2017), Hazard free green synthesis of ZnO nano-photo-catalyst using *Artocarpus heterophyllus* leaf extract for the degradation of Congo red dye in water treatment applications, Journal of Environmental Chemical Engineering https://doi.org/10.1016/j.jece.2017.05.058

Wang Y, Wang Z, Muhammad S, He J (2012) Graphite-like C3N4 hybridized $ZnWO_4$ nanorods: synthesis and its enhanced photocatalysis in visible light. Cryst Eng Comm 14:5065. https://doi.org/10.1039/c2ce25517k

Yanan D, Jiansen N, Pengfei H, Junan W, Xueling H, Hui X (2013) Synthesis and characterization of manganese doped CeO2 nanopowder from hydrolysis and oxidation of Ce37Mn18C45. J Rare Earth 31:271–275. https://doi.org/10.1016/S1002-0721(12)60271-3

Yue L, Zhang XM (2009) Structural characterization and photocatalytic behaviors of doped CeO2 nanoparticles. J Alloys Compd 475:702. https://doi.org/10.1016/j.jallcom.2008.07.096

Zhou K, Wang X, Sun X, Peng Q, Li Y (2005) Enhanced catalytic activity of ceria nanorods from well-defined reactive crystal planes. J Catal 229(1):206–212. https://doi.org/10.1016/j.jcat.2004.11.h004tkmi